Geomechanics and Engineering, *Vol. 35, No. 2 (2023) 195-208*
https://doi.org/10.12989/gae.2023.35.2.195

Experimental study on the vertical bearing behavior of nodular diaphragm wall in sandy soil based on PIV technique

Jiujiang Wu*[1,2], Longjun Pu[1], Hui Shang[1], Yi Zhang[3], Lijuan Wang[4] and Haodong Hu[1]

[1]*Shock and Vibration of Engineering Materials and Structures Key Laboratory of Sichuan Province, Southwest University of Science and Technology, No.59, Qinglong Avenue, Mianyang, The People's Republic of China*
[2]*Department of Civil and Environmental Engineering, Western University, London N6A 5B9, Canada*
[3]*Shanghai Horizon Construction Development Co., Ltd., No.1815 Huiwang Road, Shanghai, The People's Republic of China*
[4]*State Key Laboratory of GeoHazrd Prevention and GeoEnvironment Protection, Chengdu University of Technology, No.1, East 3rd Road, Erxianqiao, Chengdu, The People's Republic of China*

(*Received May 24, 2023, Revised Sptember 22, 2023, Accepted September 26, 2023*)

Abstract. The nodular diaphragm wall (NDW) is a novel type of foundation with favorable engineering characteristics, which has already been utilized in high-rise buildings and high-speed railways. Compared to traditional diaphragm walls, the NDW offers significantly improved vertical bearing capacity due to the presence of nodular parts while reducing construction time and excavation work. Despite its potential, research on the vertical bearing characteristics of NDW requires further study, and the investigation and visualization of its displacement pattern and failure mode are scant. Meanwhile, the measurement of the force component acting on the nodular parts remains challenging. In this paper, the vertical bearing characteristics of NDW are studied in detail through the indoor model test, and the displacement and failure mode of the foundation is analyzed using particle image velocimetry (PIV) technology. The principles and methods for monitoring the force acting on the nodular parts are described in detail. The research results show that the nodular part plays an essential role in the bearing capacity of the NDW, and its maximum load-bearing ratio can reach 30.92%. The existence of the bottom nodular part contributes more to the bearing capacity of the foundation compared to the middle nodular part, and the use of both middle and bottom nodular parts increases the bearing capacity of the foundation by about 9~12% compared to a single nodular part of the NDW. The increase in the number of nodular parts cannot produce a simple superposition effect on the resistance born by the nodular parts since the nodular parts have an insignificant influence on the exertion and distribution of the skin friction of NDW. The existence of the nodular part changes the displacement field of the soil around NDW and increases the displacement influence range of the foundation to a certain extent. For NDWs with three different nodal arrangements, the failure modes of the foundations appear to be local shear failures. Overall, this study provides valuable insights into the performance and behavior of NDWs, which will aid in their effective utilization and further research in the field.

Keywords: model test; nodular diaphragm wall; nodular part; PIV technology; vertical bearing behavior

1. Introduction

With the rapid growth of the global construction industry, the demand for the construction of buildings, roads, and railways is increasing, necessitating higher standards for foundation construction. However, traditional foundation techniques are becoming less effective in meeting these demands. The nodular diaphragm wall (NDW) is a novel type of foundation, which consists of a wall, middle nodular, and bottom nodular, as shown in Fig. 1. This design enhances the stability of the structure between soil layers by increasing friction between the wall and soil through the nodular parts. As a result, it maximizes the bearing capacity of the soil between walls. Research (Yokoyama *et al.* 2009) indicates that compared to traditional diaphragm walls, NDW significantly increases bearing capacity while reducing the section area and volume of the foundation, which can shorten construction time by up to 20% and reduce earth excavation by 30%. Due to its excellent engineering characteristics, NDW has been applied in constructing high-rise buildings and high-speed railways.

The Tokyo Skytree (as shown in Fig. 1), a radio tower located in Tokyo, Japan, is the tallest self-supporting tower in the world, having been completed in 2012 with a height of 634 meters. Due to the presence of many existing buildings adjacent to the radio tower foundation site, traditional pile foundation construction was deemed difficult (Watanabe *et al.* 2011). To address this challenge, a modified diaphragm wall foundation, NDW, was selected for the main base of the Tokyo Skytree, as shown in Fig. 1. NDW offers several advantages, including high construction efficiency, low noise, large overall stiffness, and excellent seismic performance. Moreover, it can be constructed near existing buildings (Wu *et al*. 2016, Wu *et al.* 2023). This resulted in the successful implementation of the first nodular diaphragm wall application in the field of foundation engineering (Watanabe *et al*. 2018). In addition, NDW has been partially applied in some high-speed railway

*Corresponding author, Professor
E-mail: wujiujiang1988@126.com

ISSN: 2005-307X (Print), 2092-6219 (Online)

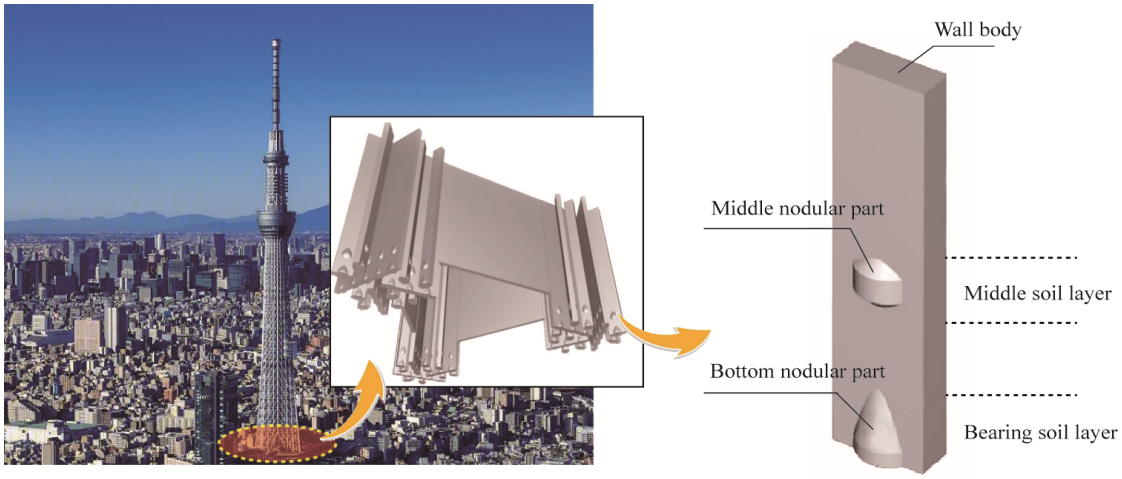

Fig. 1 Application case and structural scheme of nodular diaphragm walls (Yokoyama *et al.* 2009)

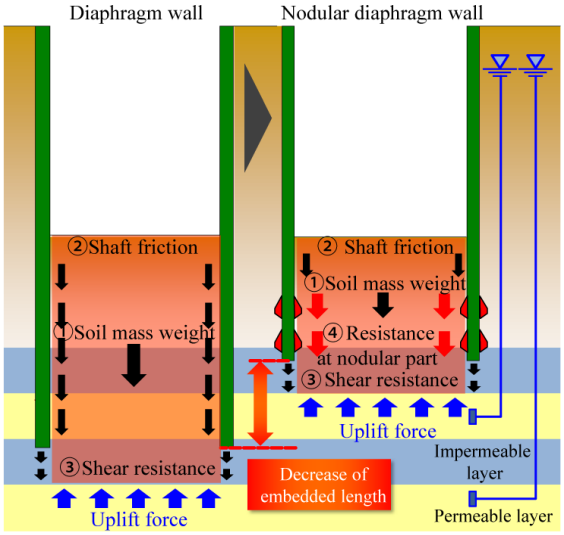

Fig. 2 Application case of nodular diaphragm walls in tunnel engineering for high-speed railway (Watanabe *et al.* 2018)

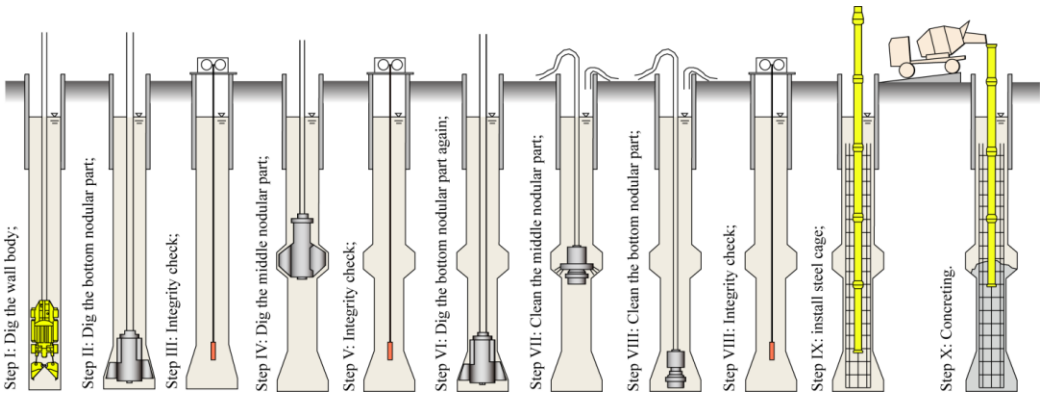

Fig. 3 Construction method of nodular diaphragm walls

and subway tunnel projects due to its superior anti-floating characteristics, as shown in Fig. 2. The construction process for NDW involves adding nodular parts to the traditional diaphragm wall technique, as shown in Fig. 3.

At present, some scholars have carried out some related studies on NDW. Watanabe *et al.* (2011) presented the construction method for the NDW foundation of a new type of high-rise building and conducted compressive and uplift tests on-site, which showed that the nodular part significantly improved the vertical bearing capacity of the NDW. Watanabe *et al.* (2018) investigated the uplift resistance of the NDW in comparison with conventional diaphragm wall through field tests and centrifugal model tests, demonstrating that the presence of the nodular part

significantly enhanced the uplift resistance of the foundation. Meanwhile, many scholars have conducted indoor model tests, field loading tests, and numerical simulations to investigate the characteristics of pile foundations with nodular/belled parts, such as bell-shaped piles, under-reamed piles, pre-bored grouted planted piles with enlarged grout bases, as well as nodular pile foundations, etc. These investigations focused on their uplift capacity (Emirler *et al.* 2015, Qian *et al*. 2019, Yang and Qiu 2020, Al-Bayati *et al.* 2023, Cheraghi and Ghorbani-Tanha 2023), axial bearing capacity (Zhou *et al.* 2019, Majumder and Chakraborty 2021a, b, Zhou *et al.* 2021, Jala *et al*. 2022, Yu *et al*. 2022) and lateral capacity (Qian *et al.* 2020, Majumder and Chakraborty 2022) in engineering practice and proposed calculation methods for uplift capacity and settlement of such piles. The investigations revealed that the presence of nodular or belled parts positively contributed to improving the bearing capacity of pile foundations. It is worth noting that the bearing behavior of NDWs tends to be complex due to their unique construction and structure, which differs from the common pile foundations with nodular/belled parts. Therefore, the research findings on piles cannot be simply applied to the NDWs. However, they can provide valuable references and inspiration.

Although the NDW has been partially applied in Japan and relevant experimental studies have been conducted, in-depth investigations on the load transfer mechanism and failure modes of NDW are scarce, and its bearing capacity calculation is empirical and still based on nodular piles. Additionally, the limited research on the displacement pattern, failure mode visualization, and the challenging measurement of the force components acting on the nodular parts highlights the need for further exploration of the vertical load-bearing properties and deformation failure modes of the NDW. In this paper, the vertical bearing characteristics of NDW in sandy soil are studied in detail through the indoor PIV model test. Three types of NDWs are examined, encompassing those with a sole bottom nodular part, a single middle nodular part, and configurations with both middle and bottom nodular parts. Initially, we elucidate the testing principles and methodologies, with a specific focus on detailing the PIV technology setup and the monitoring and computation of the forces acting on the nodular components. Following this, we present the experimental results, covering critical aspects such as the Q-s curves for the three foundational types, axial force and kin friction, nodular resistance, load-sharing ratios, etc. The special attention is directed towards explicating the foundational displacement behavior and failure modes. The findings of this paper offer valuable insights into the performance and behavior of NDWs, potentially contributing to their effective utilization for future research in the field.

2. Overview of the model test

2.1 Design and setup of NDW models

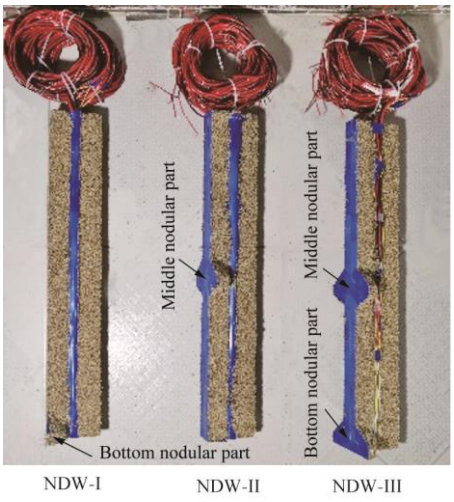

(a) half model

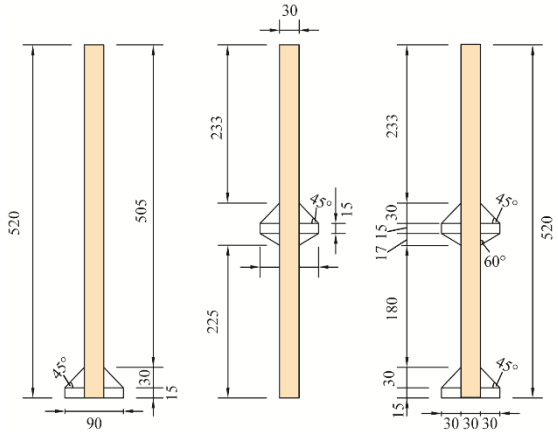

(b) dimension size (units: mm)

Fig. 4 Nodular diaphragm wall models

Based on the prototype diaphragm wall with a unit trench length of 4.8 m and a width (or wall thickness) of 0.9 m, the similarity ratio of the experimental model is set to be 1:30. To investigate the effects of different nodular part positions on the vertical bearing characteristics of the NDW, three types of NDW models were investigated: NDW-I (with a bottom nodular part only), NDW-II (with a middle nodular part only), and NDW-III (with middle and bottom nodular parts), as shown in Fig. 4.

The form of the "half model" foundation (Fig. 4(a)) has been established for the experiment, which will utilize PIV (Particle Image Velocimetry) technology to observe the displacement and failure modes of the NDW. A unit trench length of 80 mm and a width of 30 mm for the NDW model have been determined. The nodular parts have also been appropriately enlarged based on a constructional investigation of the nodular part to make the experimental phenomena more visible and easier to capture.

Based on the published experience in conducting model tests of the diaphragm wall foundations (Wu et al. 2016), the similarity materials for the NDW were made of plexiglass. To simulate the roughness of the concrete

(a) test setup

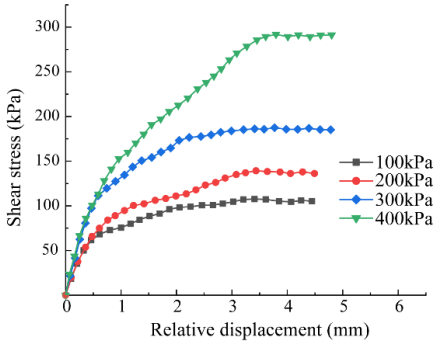

(b) test result

Fig. 5 Direct shear test of wall-soil interface

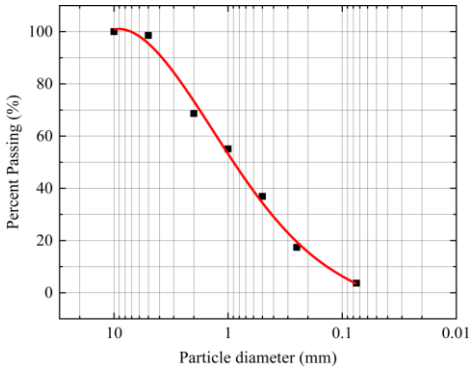

Fig. 6 Particle size distribution curve

Table 1 Physical and mechanical parameters of soil

Soil sample	Density (g/cm^3)	Cohesion (kPa)	Internal friction angle (°)	Water content (%)	Compression modulus (MPa)
Fine sand	1.745	0	36	2.813	9.5

surface, a layer of sand is glued on the plexiglass surface, as shown in Fig. 4. The particle size and intensity of the sand adhered to the model walls will directly impact the wall-soil interface. The appropriate particle size and intensity can be determined using the direct shear testing test based on the result of the wall-soil interfacial angle, as shown in Fig. 5. Finally, it can be found that standard sand of 0.5~1.5 mm diameter with a density of 50~70 grains per square centimeter yields the ideal results. In this scenario, the internal friction angle of the wall-soil interface is set at 0.86 of the internal friction angle of the sand used in the test. This setting aligns with the actual working conditions of the interface between concrete and soil.

2.2 Soil property and sensor arrangement

The soil model used in the experiment is sandy soil, and its physical and mechanical parameters are listed in Table 1. The particle size distribution curve is shown in Fig. 6.

The sensors used in this model test mainly include dial

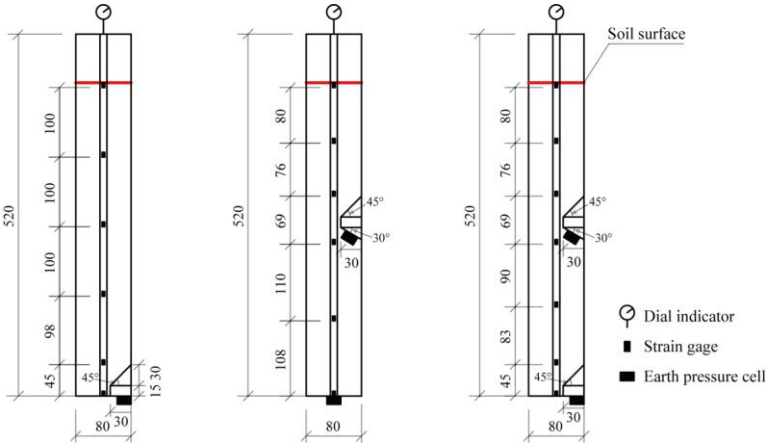

Fig. 7 Layout of testing sensors (units: mm)

indicators, strain gauges, and earth pressure cells. The dial indicator is placed at the top of the model wall to measure displacement variations during loading. Strain gauges are symmetrically arranged on both sides of the wall to analyze changes in axial force and skin friction. Earth pressure cells are mainly located at the end of the wall and below the nodular part to assist the strain gauges in analyzing the load-bearing and changes in axial force and skin friction at the nodular part. The specific sensor layout is depicted in Fig. 7.

The testing principle for nodular part resistance involves the use of earth pressure cells placed evenly below the nodular parts. Prior to loading, initial data is collected by taking readings from the earth pressure cells. During loading, the earth pressure cell readings are taken at each load level, and the initial data is subtracted to obtain the average soil pressure acting on each nodular part. The obtained soil pressure is then multiplied by the contact area between the nodular part and soil to obtain the converted soil resistance acting on the nodular part. The vertical component of the converted soil resistance is considered as the load acting on the nodular part.

Specifically, the value of the total resistance of the wall section where the middle nodular part is located can be obtained as F_1

$$F_1 = \frac{EA}{a}\sum_{i=1}^{a}\varepsilon_i - \frac{EA}{b}\sum_{j=1}^{b}\varepsilon_j \tag{1}$$

where ε_i and ε_j are the strain values of the strain gages immediately upper side and down the middle nodular part, respectively; E is the elasticity modulus of the NDW; A is the horizontal non-nodular cross-sectional area of the NDW; i = 1, ..., a, and j = 1, ..., b; a and b are the number of corresponding strain gauges, respectively.

By installing the earth pressure cell, the value of earth pressure above the middle nodular part Q_1 can be deduced as:

$$Q_1 = \frac{A_1}{c}\sum_{l=1}^{c} p_l \tag{2}$$

where A_1 is the total area of the tapered surface above the middle nodular part protruding on both sides, and p_l is the value of the earth pressure captured by the earth pressure cell above the middle nodular part, l =1, ..., c; c is the corresponding number of earth pressure cells.

Based on the equilibrium of forces in the vertical direction in the middle nodular part, F_1 is subtracted from the vertical component of the value Q_1 to obtain the mean skin friction value f_1 within the middle nodular part

$$f_1 = \frac{F_1 - Q_1\cos\theta_1}{A_2} \tag{3}$$

where A_2 is the area of the wall section on either side of the middle nodular part (i.e., the horizontal cross-section area excluding the nodular part), θ_1 is the surface inclination of the nodular part.

Similarly, the total resistance of the wall section where the bottom nodular part is located F_2 can be obtained as

$$F_2 = \frac{EA_3}{d}\sum_{m=1}^{d}\varepsilon_m - \frac{A_3}{e}\sum_{n=1}^{e} p_n \tag{4}$$

where ε_m is the strain value measured at the upper part of the bottom nodular part; p_n is the value of earth pressure collected at the bottom of the NDW; A_3 is the area of the NDW's bottom; m = 1, ..., d, and n = 1, ..., e; m and n is the number of corresponding strain gauge and earth pressure cell, respectively.

At this point, the mean skin friction value f_2 within the bottom nodular part:

$$f_2 = \frac{F_2}{A_4} \tag{5}$$

where A_4 is the area of the wall section on either side of the bottom nodular part (i.e., the horizontal cross-section area excluding the nodular part).

According to the above steps, we can estimate the soil resistance and skin friction of the middle and bottom nodular parts of the NDW. At this point, the load transfer mechanism, including the load-sharing ratio of the nodular part, can be analyzed in detail.

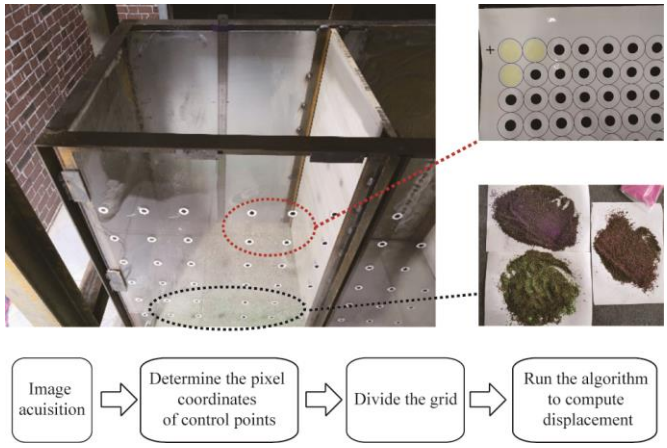

Fig. 8 PIV setup and operation steps

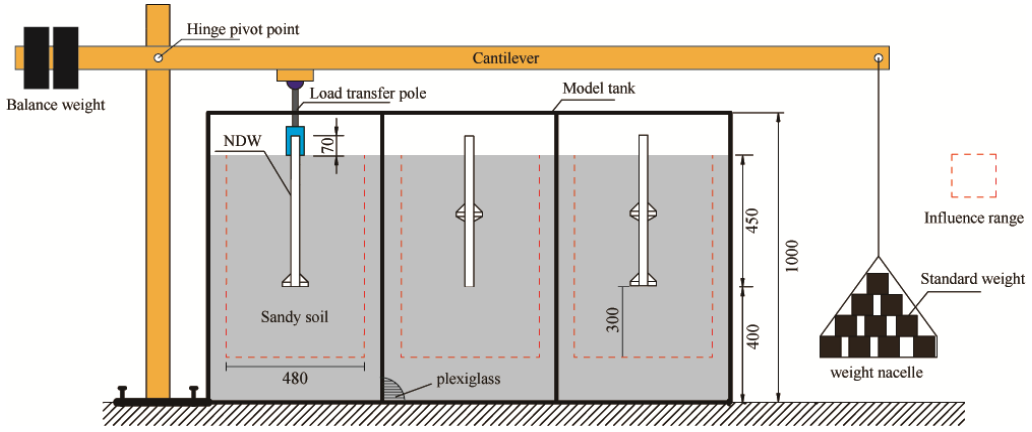

Fig. 9 Loading device and scheme (units: mm)

2.3 PIV setup and loading scheme

Particle image velocimetry (PIV) is an image analysis technique that has been rapidly advancing. Its application in geotechnical engineering was first introduced by White *et al.* (2003), and later an open-source procedure called GeoPIV-RG was developed by combining MATLAB with PIV-related characteristics. The PIV technique has been applied in the field of geotechnical engineering to measure the variation of the displacement of a single pile after horizontal loads, as well as the area of vertical and horizontal displacements of the surrounding soil. (Al-Neami *et al.* 2022). This model test utilized the GeoPIV-RG procedure to analyze the soil deformation characteristics around the NDW during the loading process. According to the GeoPIV-RG procedure's operation steps, the corresponding PIV technology image acquisition system should include the following major elements.

(1) tracer particles: after repeated testing, a mixture of 20-30 mesh-sized light green sand and river sand in a 1:2 ratio was found to be the most effective tracer particles (see Fig. 8);

(2) control points: 8 rows of 6 columns of special stickers, consisting of 10mm diameter black circles and 20 mm white circle stickers, were posted in the observation window to create control points while avoiding the position of the model wall (see Fig. 8);

(3) Light source: multiple 30W floodlights were arranged symmetrically to provide a stable light source for the test;

(4) CCD high-definition digital camera: a Canon EOS 80D high-definition digital camera was used for the model experiment.

An effective lever-loading system was designed for this model test, providing solid stability and high operability, as shown in Fig. 9. This system enables the compressive load to be applied to each of the three NDW model walls in sequence. A counterweight is placed at the left end of the lever to balance the self-weight of the cantilever. As the required load in this experiment is relatively small, measurable and regular sintered bricks are used instead of metal weights. These bricks are gradually added to the nacelle located on the right side of the lever system during the loading process. The loading levels are set to be 10-15 levels until the ultimate bearing capacity of each NDW model is reached. Additionally, the boundary conditions of the models are carefully regulated and designed. Specifically, we consider the influence range of the model in the horizontal direction to be within three times the maximum side length of the periphery of the diaphragm

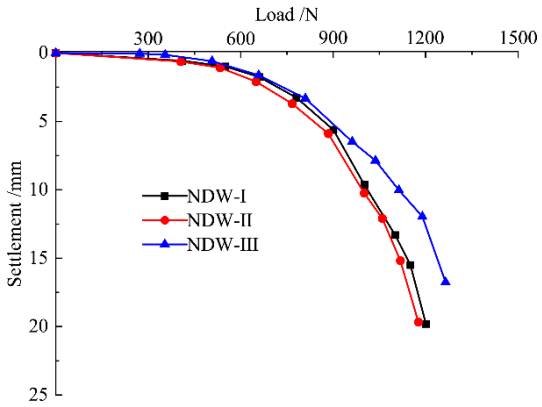

Fig. 10 *Q-s* curves

wall, which amounts to 480 mm. Simultaneously, for the vertical direction, we determine the influence range based on the thickness of the compressed soil layer, estimated through settlement calculations (Wu *et al.* 2015). As deduced from the calculations, this vertical influence range is determined to be 300 mm.

3. Experimental results

3.1 Load transfer analysis

3.1.1 Q-s curves

Fig. 10 depicts the load-displacement relationship (*Q-s* curves) of the three types of NDWs. It is worth noting that during the last loading level, all three types of foundations experienced destabilization and produced large displacements, which exceeded the range of the measuring instruments. Therefore, the corresponding displacement points were not included in the *Q-s* curves.

At the early loading stage, the *Q-s* curves for the three NDW foundations showed consistent trends. However, as the loads increased to over 900 N, differences became noticeable. Under the same loading conditions, the displacements (or settlements) of NDW-I (with only a bottom nodular part, as shown in Fig. 4) and NDW-II (with only a middle nodular part) were similar, but both were larger than those of NDW-III (with both middle and bottom nodular parts). Since all three foundation types have the same section size, except for the nodular part, the position and number of nodular parts are the only factors that differ. This indicates that the position of the nodular part, especially the number, has a significant effect on the foundation *Q-s* curve, particularly under larger loads. The settlement of the foundation with more nodular parts (i.e., NDW-III) is significantly smaller, while the settlement of the foundation with only a bottom nodular part (i.e., NDW-I) is slightly smaller than that of the foundation with only a middle nodular part (i.e., NDW-II).

For ease of comparison, the load corresponding to 15 mm of settlement is taken as the ultimate bearing capacity for the three foundation types. The ultimate bearing capacity of NDW-I is determined to be 1142.9 N, NDW-II is 1114.3 N, and NDW-III is 1248.9 N. The ultimate bearing capacity of NDW-III is increased by 9.27% and 12.08% compared to NDW-I and NDW-II, respectively. These results indicate that, under the same wall section size and depth, the ultimate load capacity of the NDW foundation with only a bottom nodular part (NDW-I) is slightly greater than that of the NDW foundation with only a middle nodular part (NDW-II), but both are lower than the NDW foundation with both middle and bottom nodular parts (NDW-III). In general, the presence of a bottom nodular part contributes more to the improvement of the foundation's bearing capacity compared to a middle nodular part. Additionally, the simultaneous use of both middle and bottom nodular parts in NDW-III results in a certain degree of increment in the bearing capacity of the foundation compared to the use of a single nodular part in NDW-I and NDW-II, but the effect was not significant.

3.1.2 Analysis of axial force and skin friction

Fig. 11 displays the axial force curves of the three types of NDW foundations distributed along the depth. As shown in Fig. 11(a), for NDW-I with only a bottom nodular part, the load on the wall top is transmitted up and down through the wall to the bottom under all loading levels. With the relative displacement between the wall and soil, the wall generates skin friction in the opposite direction of the downward pressure. As the upper load develops, the wall resistance gradually increases, thus offsetting a part of the downward pressure and decreasing the axial force.

Fig. 11(b) displays the axial force curves of NDW-II with only a middle nodular part, where the axial force gradually decreases with the wall depth at all loading levels due to skin friction. In addition, the middle nodular part (ranging from 0.235 to 0.305 m of the wall depth) provides resistance to the wall, which is subjected to both the pressure from the upper wall and the skin friction in the upward direction on the outside of the wall. As a result, the axial force of NDW-II decreases more significantly than that of NDW-I within this range, leading to a significant change in the axial force curve in this depth range where the middle nodular part is located, much greater than the change in the rest of the depth range. As shown in Fig. 11(c), the axial force distribution pattern of NDW-III is similar to that of NDW-II, and its axial force curve also changes significantly in the middle of the wall under the influence of the middle nodular part.

Overall, the axial force of all three NDW foundations decreases with depth at all loading levels due to the combined influence of skin friction and nodular part resistance, with the decreasing range increasing as the load increases. Furthermore, the axial force curves of the NDW foundations change significantly due to the presence of the middle nodular part. To further analyze the load transfer mechanism of the foundation, the skin friction distribution curves along the wall for the three types of NDW foundations at various loading levels should be investigated.

Fig. 12 illustrates that the skin friction of NDW foundations is affected by the degree of exertion and varies with depth for all loading levels. As the load level increases, the skin friction also increases gradually. However, when the load is very high, the rate of increase in skin friction slows down and eventually reaches a stable value within a certain depth range. This suggests that the skin friction has reached a satisfactory level and tends towards an ultimate value. In general, the distribution of skin friction is similar across the

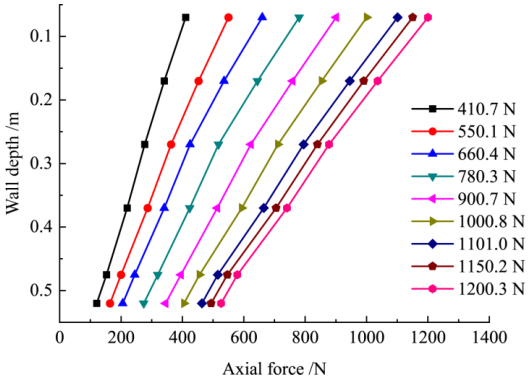

(a) NDW-I

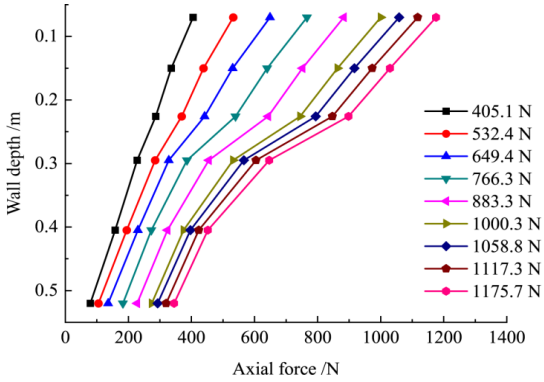

(b) NDW-II

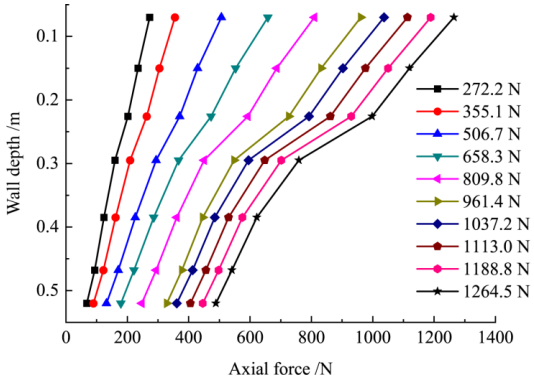

(c) NDW-III

Fig. 11 Axial force distribution curves

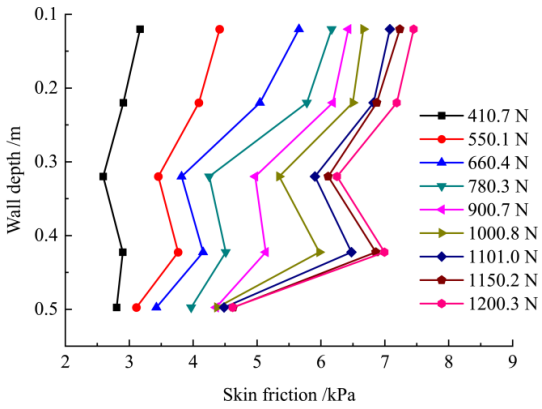

(a) NDW-I

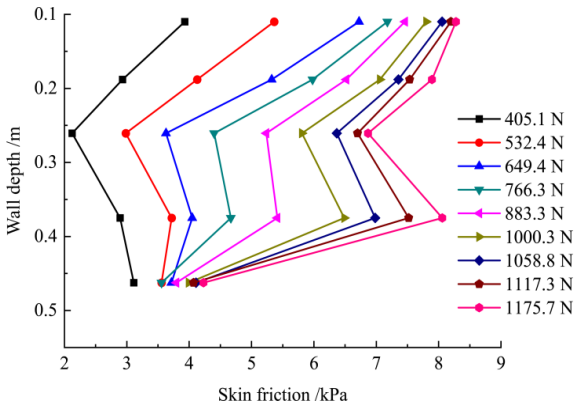

(b) NDW-II

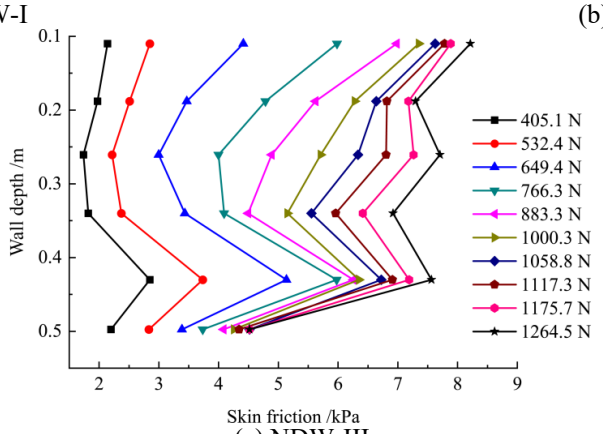

(c) NDW-III

Fig. 12 Skin friction curves

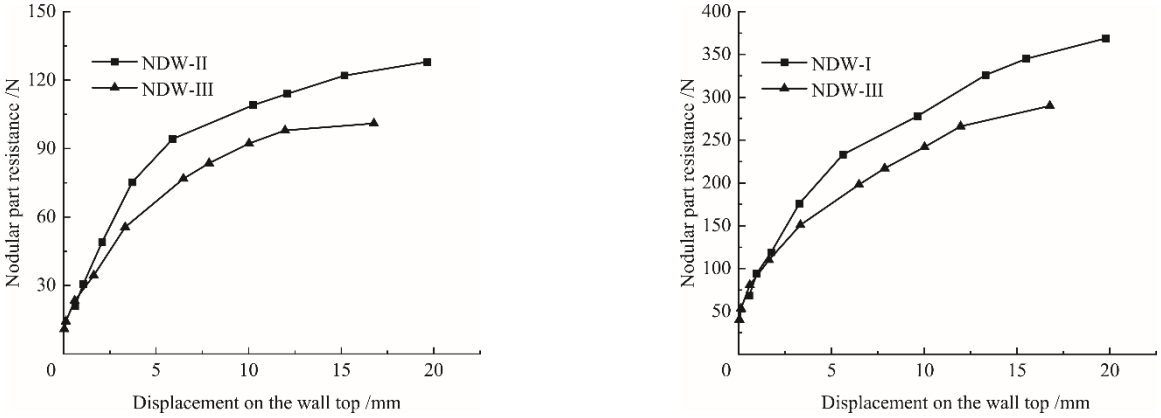

(a) middle nodular part (b) bottom nodular part

Fig. 13 Forces analysis acting on the nodular parts

three types of NDW foundations. The position or number of nodular parts has little impact on the exertion and distribution of skin friction for NDW foundations.

3.1.3 Nodular part resistance analysis

In order to study the forces acting on the nodular parts, the development and changes in nodular part resistance for the three types of NDW foundations were recorded and analyzed separately. Figure 13 shows the forces at the same nodular part positions for the middle and bottom nodular parts of NDW-I, NDW-II, and NDW-III, which were compared and analyzed to gain insights into the forces acting on the nodular parts in different foundation categories and to understand how they vary with the nodular part arrangement.

Fig. 13 illustrates that the nodular part resistance gradually increases with displacement on the wall top for both middle and bottom nodular parts, exhibiting an initial linear growth stage followed by a slower non-linear growth trend as the load increases. In general, the nodular part resistance shows a hyperbolic variation pattern with increasing displacement. Comparing Fig. 13(a) to Fig. 13(b), it is apparent that NDW-III, with both types of nodular parts, has lower nodular part resistance than NDW-I and NDW-II, which have only one type of nodular part. For instance, under the same displacement on the wall top, the middle nodular part resistance of NDW-II is higher than that of NDW-III (Fig. 13(a)), and the bottom nodular part resistance of NDW-I is higher than that of NDW-III (Fig. 13(b)). This indicates that the presence of multiple nodular parts limits the effectiveness of nodular resistance. Specifically, increasing the number of nodular parts does not simply add up the resistance borne by the nodular parts but results in a certain discount. This is also one of the reasons why the load-bearing capacity of NDW-III is not significantly improved compared to NDW-I and NDW-II.

Upon comparing Figs. 13(a) and 13(b), it is clear that the resistance of the bottom nodular part is significantly greater than that of the middle nodular part for the same displacement on the wall top. In the case of NDW-III, at the last level of loading, the resistance of the bottom nodular part reaches 290 N, while the resistance of the middle nodular part is only 101 N. At the ultimate loading level, the resistance of the bottom nodular part is approximately 2.87 times higher than that of the middle nodular part. This phenomenon can be attributed to the fact that the bottom nodular part has a much larger force area than the middle nodular part under vertical pressure, resulting in a greater resistance compared to the middle nodular part.

3.1.4 Load-sharing ratio analysis

Fig. 14 presents the load-sharing ratios of nodular part resistance, bottom resistance, and skin friction for the three NDW foundations. In Fig. 14(a), it can be observed that the sharing ratio of skin friction for NDW-I (with only a bottom nodular part) gradually decreases with the increasing load, but it remains consistently high and exceeds 50% throughout the entire loading process. Furthermore, the sharing ratios of bottom resistance and nodular part resistance increase with the increasing load, with the sharing ratio of bottom resistance slightly larger than that of nodular part resistance. These observations indicate that friction dominates the behavior of the NDW-I foundation during the loading process, and the load-sharing ratio of the nodular part remains below 30% throughout the entire loading process.

Fig. 14(b) shows that the sharing ratio of skin friction for NDW-II (with only a middle nodular part) gradually decreases during the entire loading process, but it remains consistently high, with all values exceeding 55%. Additionally, the sharing ratio of bottom resistance and nodular part resistance increases with the increasing load, with the sharing ratio of bottom resistance larger than that of nodular part resistance. These observations suggest that friction dominates the behavior of the NDW-II foundation during the loading process, with relatively small load sharing between nodular part resistance and bottom resistance. The maximum sharing ratio of nodular part resistance does not exceed 30%, while that of bottom resistance is less than 20%.

Fig. 14(c) shows that the sharing ratio of skin friction for NDW-III (with both middle and bottom nodular parts) gradually decreases during the entire loading process, with none of the load-sharing ratios exceeding 50%. However, the sharing ratio of bottom resistance and nodular part resistance (including middle and bottom nodular part resistance) increases with the increasing load, with the sharing ratio of

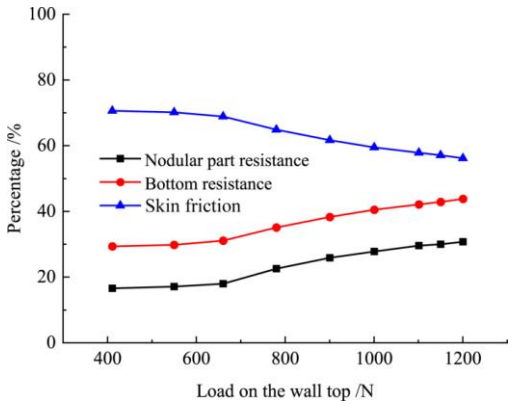

(a) NDW-I

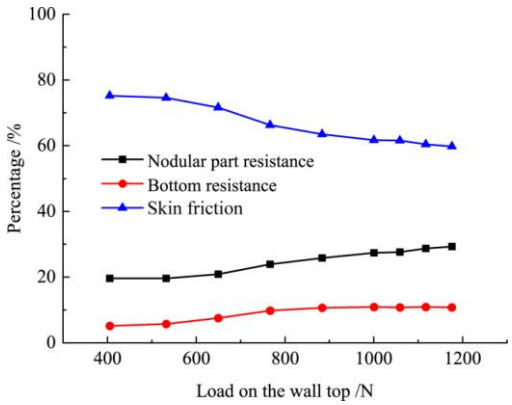

(b) NDW-II

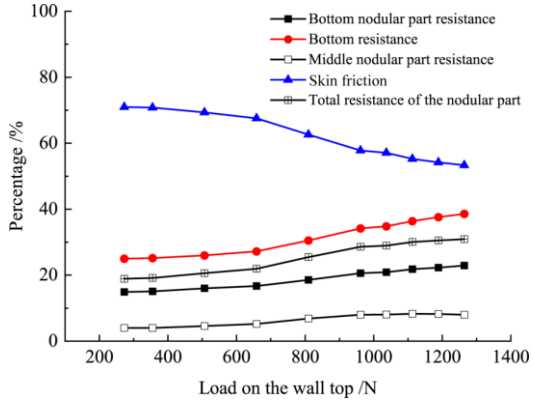

(c) NDW-III

Fig. 14 Load sharing ratios

bottom resistance larger than that of nodular part resistance. Among the nodular part resistance, the sharing ratio of the middle nodular part resistance is smaller than that of the bottom nodular part resistance. The maximum sharing ratio of bottom nodular part resistance is 22.9%, while the maximum sharing ratio of middle nodular part resistance is 8.02%, and the maximum sharing ratio of total nodular part resistance is 30.92%.

In general, it can be observed that skin friction is the main factor contributing to the bearing capacity of the three types of NDW foundations throughout the loading process. Meanwhile, the nodular part plays an essential role in the bearing capacity of the NDW, and its maximum load-bearing ratio can reach 30.92%, which is not decisive. This further confirms the conclusion drawn in Section 3.1 that the combined use of the middle and bottom nodular part can enhance the foundation's load-bearing capacity, but the improvement effect is not significant.

3.2 Displacement and failure modes analysis

3.2.1 Displacement distribution

During the loading process of the three NDW foundations, images were captured and input into the GeoPIV-RG procedure for displacement field analysis using the PIV technique (see Section 2.3). The results of the analysis are presented in Figs. 15-17, which show the soil displacement contour and vector distribution around the three NDWs under specific loading levels. Fig. 15(a) indicates that the soil displacement around NDW-I (which only has a bottom nodular part) is concentrated mainly at the nodular part and gradually spreads downward radially. The displacement vector diagram in Fig. 15(b) confirms that the soil around the wall produces a larger displacement vector field at the nodular part of the foundation, especially in the downward direction at the bottom.

Fig. 16(a) shows that for NDW-II (which has a middle nodular part only), the soil displacement around the wall is concentrated mainly in the middle nodular part and the bottom of the wall. The displacement gradually spreads around and below the wall. The displacement vector diagram in Fig. 16(b) confirms that the soil around the wall generates a larger displacement vector field in the nodular part and the bottom of the wall, especially below the middle nodular part. By comparing Fig. 15(a) with Fig. 16(a), it can be seen that the influence range of vertical soil displacement of NDW-I is significantly larger than that of NDW-II due to the presence of the bottom nodular part. However, the soil disturbance range of the middle part of NDW-II is significantly larger than that of NDW-I due to the presence of the middle nodular part of NDW-II.

Fig. 17(a) shows that for NDW-III (which has middle and bottom nodular parts), the soil displacement around the wall is mainly concentrated at the middle and bottom nodular parts. The displacement gradually spreads around and below the wall. The displacement vector diagram in Fig. 17(b) confirms

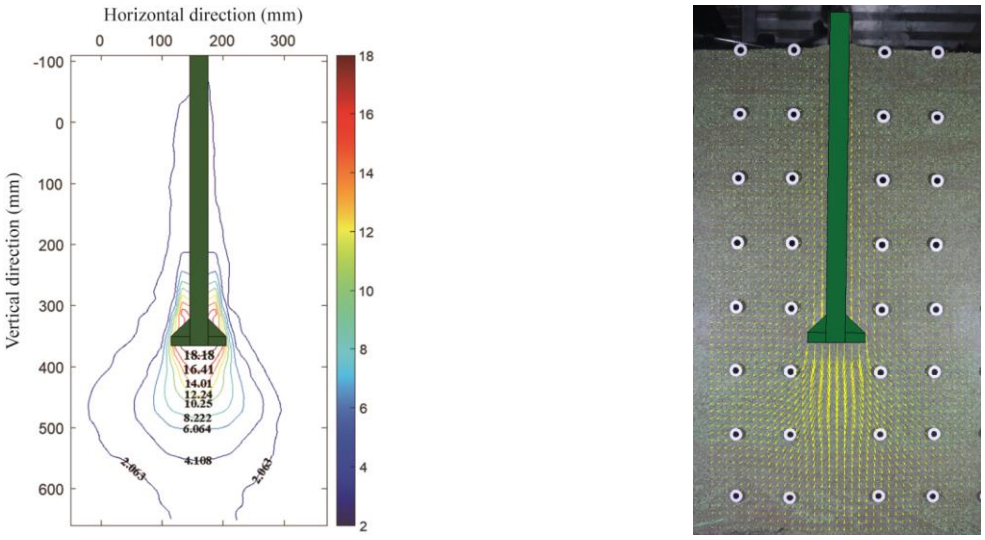

(a) displacement contour (b) displacement vector

Fig. 15 Displacement distribution (NDW-I)

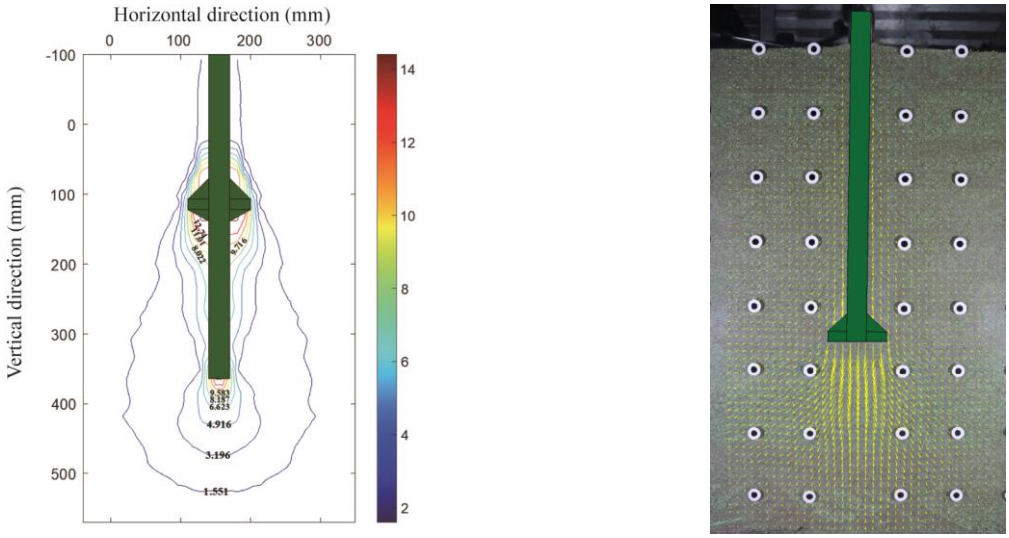

(a) displacement contour (b) displacement vector

Fig. 16 Displacement distribution (NDW-II)

that the soil around the wall produces a large displacement vector field mainly at the position of the middle nodular part of the foundation and the bottom of the wall, especially below the bottom nodular part.

By comparing Figs. 15(a), 16(a) with 17(a), it can be observed that the soil displacement influence range of NDW-III is significantly larger, especially in the depth range of this wall from the middle nodular part to the bottom. This indicates that the presence of the nodular parts changes the displacement field of the soil around NDW and increases the displacement influence range of the foundation in the vertical and lateral directions to some extent. By comparing Figs. 15(b), 16(b) with 17(b), it can be noticed that the nodular part has an influence on the NDW displacement vector field. Specifically, the presence of the nodular part mobilizes more soil around the wall to work together, and this behavior is more pronounced for NDW-III, contributing to the enhancement of its load-bearing characteristics.

3.2.2 Analysis of failure modes

Fig. 18 shows the maximum shear strain distribution of the soil around the foundation under ultimate load for the three types of NDW foundations. It should be noted that the maximum shear strain distribution is commonly used to analyze the failure modes and forms of the foundation (Wu *et al.* 2017).

It can be seen from Fig. 18(a) that the maximum shear strain values for the NDW-I (with a bottom nodular part only) under ultimate load are primarily concentrated near the bottom nodular part, particularly at the upper and lower edges of the nodular part. This is specifically indicated by the formation of a shear rupture surface with wedge extensions upwards at the edge of the bottom nodular part, as well as a shear rupture surface downwards at the edge of the bottom nodular part. For the NDW-I, the failure mode is characterized by local shear failure (Chen *et al.* 2020), which is generated along the periphery of the bottom nodular part.

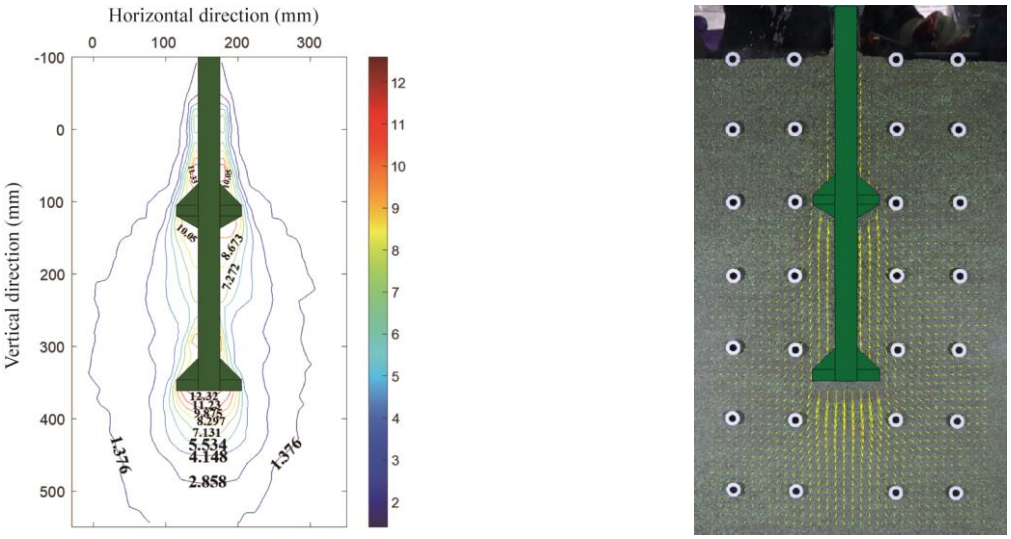

(a) displacement contour (b) displacement vector

Fig. 17 Displacement distribution (NDW-III)

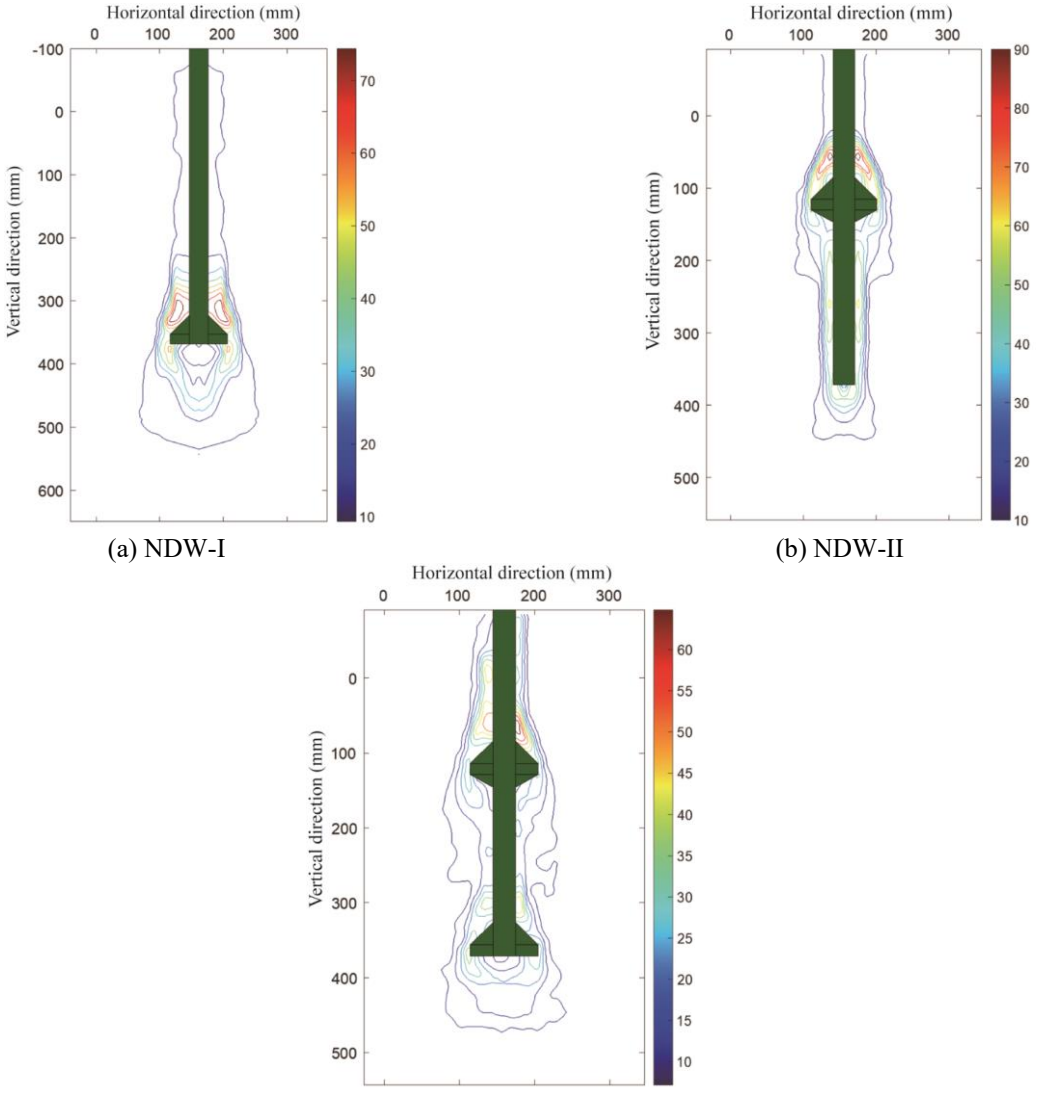

(a) NDW-I (b) NDW-II

(c) NDW-III

Fig. 18 Maximum shear strain distribution

4. Conclusions

In this study, an in-depth investigation into the vertical bearing characteristics of NDW foundations, representing a novel and promising foundation type, was conducted based on indoor PIV model tests. The following conclusions can be drawn from the findings:

• Comparison of Foundation Types: When evaluating the ultimate bearing capacity under identical wall section size and depth conditions, it was observed that the foundation with only a bottom nodular part exhibited slightly better performance compared to the one with just a middle nodular part. However, it is noteworthy that both of these configurations yielded lower bearing capacities than the foundation incorporating both middle and bottom nodular parts, thus highlighting the substantial contribution of the bottom nodular part to the overall bearing capacity, surpassing that of the middle nodular part. The utilization of both middle and bottom nodular parts resulted in an approximately 9~12% increase in bearing capacity compared to a foundation with a single nodular part.

• Axial Force Behavior: Throughout the various loading levels, a consistent decrease in axial force for all three NDW foundation types with increasing wall depth was noted. This decline was attributed to the combined effects of skin friction and nodular resistance, with a more pronounced rate of reduction observed as the applied load increased. Significantly, the presence of the middle nodular part had a notable influence on the axial force curve, demonstrating the importance of nodular arrangements in affecting load-bearing behavior. However, the distribution of skin friction remained similar in form across all three NDW types, with the position and quantity of nodular parts having limited impact on skin friction distribution.

• Nodular Resistance: The research unveiled that multiple nodular parts on the NDW foundation imposed certain limitations on nodular resistance. Adding more nodular parts did not lead to a straightforward cumulative effect on resistance; instead, a discounting mechanism was introduced. Furthermore, due to variations in their contact area with the soil, the bottom nodular part exhibited significantly higher resistance compared to the middle nodular part when subjected to equivalent loading conditions.

• Role of Skin Friction and Nodular Part: The contribution of skin friction to the bearing capacity of the three foundation types was found to be substantial across the entire loading process. Simultaneously, the nodular part emerged as a critical component, with a maximum load-bearing ratio of up to 30.92 %. Importantly, the presence of the nodular part had a profound impact on the displacement field of the surrounding soil, resulting in an expanded influence of the foundation on both vertical and lateral displacement ranges.

• Failure Modes: The analysis of failure modes revealed consistent patterns for all three NDW foundation types. Failures primarily occurred as local shear failures, with rupture surfaces forming as upward wedges along the edges of the nodular parts. Additionally, localized rupture surfaces were observed to extend downward along these edges.

These findings collectively contribute valuable insights into the performance and behavior of NDW foundations, shedding light on their strengths and areas for improvement. Such insights will undoubtedly inform and benefit future research endeavors in this field and offer practical guidance for engineering applications. However, it's essential to acknowledge certain inherent limitations, including the variation in particle sizes, which are partly due to challenges posed by observation techniques and sample preparation. Future work should involve a more careful consideration of particle size distribution and exploration of methods to improve the representation of real-world soils in scaled models. Additionally, the feasibility of employing centrifuge tests or on-site experiments will be explored to enhance the research validity.

Acknowledgments

This research is supported by the National Nature Science Foundation of China (Grant No. 42007247), National Foreign Expert Project (No. DL2023036001L), Nature Science Foundation of Sichuan Province (No. 2022NSFSC1151), Scientific and Technological Innovation Projects of Housing and Urban-rural Construction in Sichuan Province (No. SCJSKJ2022-09) as well as Selected Funding of Scientific and Technological Activities for Oversea Talents in Sichuan.

References

Al-Bayati, A.W., AL-Neami, M. and Rahil, F.H. (2023), "Experimental work on the effect of under-reamed pile geometry on the pullout capacity of sand", *Int. J. Eng.*, **36**(9), 1645-1651. https://doi.org/10.5829/ije.2023.36.09c.08.

Al-Neami, M.A., Al-Dahlaki, M.H. and Al-Majidy, A.H. (2022), "Investigation of laterally loaded pile response and cohesionless soil deformation pattern using PIV technique", *Geotech. Eng. Sustain. Constr.*, 423-434. https://doi.org/10.1007/978-981-16-6277-5_34.

Chen, Y., Deng, A., Lu, F. and Sun, H. (2020), "Failure mechanism and bearing capacity of vertically loaded pile with partially-screwed shaft: experiment and simulations", *Comput Geotech*., **118**, 103337. https://doi.org/10.1016/j.compgeo.2019.103337.

Cheraghi, A. and Ghorbani-Tanha, A.K. (2023), "Numerical analysis of an innovative expanding pile under static and dynamic loading", *Geomech. Eng.*, **32**(4), 453-462. https://doi.org/10.12989/gae.2023.32.4.453.

Emirler, B., Tolun, M. and Laman, M. (2015), "Experimental investigation of the uplift capacity of group anchor plates embedded in sand", *Geomech. Eng*., **11**(5), 691-711. https://doi.org/10.12989/gae.2016.11.5.691.

Jala, S. K., Rawat, S. and Gupta, A.K. (2022), "Effect of underreamed pervious concrete columns on load-carrying capacity of loose cohesionless soils", *Int. J. Geomech*., **23**(3), 04022304. https://doi.org/10.1061/IJGNAI.GMENG-7659.

Majumder, M. and Chakraborty, D. (2021a), "Effects of scour-hole depth on the bearing and uplift capacities of under-reamed pile in clay", *Ocean Eng*., **240**, 109927. https://doi.org/10.1016/j.oceaneng.2021.109927.

Majumder, M. and Chakraborty, D. (2021b), "Bearing and uplift capacities of under-reamed piles in soft clay underlaid by stiff clay using lower-bound finite element limit analysis", *Front Struct. Civ. Eng*., **15**, 537-551. https://doi.org/10.1007/s11709-021-0708-x.

Majumder, M. and Chakraborty, D. (2022), "Under-reamed pile-soil interaction in sand under lateral loading: a three-

dimensional numerical study", *Ocean Eng*., **263**, 112398. https://doi.org/10.1016/j.oceaneng.2022.112398.

Qian, Z., Lu, X. and Yang, W. (2019), "Comparative field tests on straight-sided and belled piers on sloping ground under combined uplift and lateral loads", *J. Geotech. Geoenviron*., **145**(1), 04018099. https://doi.org/10.1061/(ASCE)GT.1943-5606.0001991

Qian, Z., Lu, X. and Yang, W. (2020), "Comparative lateral load field tests on straight-sided and belled piers in sloped ground", *Geotech. Eng*., **173**(1), 70-80. https://doi.org/10.1680/jgeen.18.00151.

White, D.J., Take, W.A. and Bolton, M.D. (2003), "Soil deformation measurement using particle image velocimetry (PIV) and photogrammetry", *Géotechnique*., **53**(7), 619-631. https://doi.org/10.1680/geot.2003.53.7.619.

Wu, J., Cheng, Q., Wen, H. and Cao, J. (2015). "Comparison on the vertical behavior of lattice shaped diaphragm wall and pile group under similar material quantity in soft soil'', *KSCE J. Civ. Eng*., **19**(7), 2051-2060. https://doi.org/10.1007/s12205-015-0367-3

Wu, J., Cheng, Q., Wen, H., Wang, L., Li, Y. and Zhang, J. (2016), "A load transfer approach to rectangular closed diaphragm wall", *P I Civil Eng-Geotec*., **169**(6), 509-526. http://dx.doi.org/10.1680/jgeen.15.00156.

Wu, J., Wang, L. and Cheng, Q. (2017), "Soil arching effect of lattice-shaped diaphragm wall as bridge foundation", *Front Struct. Civ. Eng*., **11**(4), 446-454. https://doi.org/10.1007/s11709-017-0397-7

Wu, J., Wang, L. and Cheng, Q. (2023), "Numerical modeling of current-induced scour around multi-wall foundation using large-eddy simulation", *Front Struct Civ Eng*., **17**, 546-565. https://doi.org/10.1007/s11709-023-0943-4.

Watanabe, K., Mitsumori, A., Nishioka, H. and Koda, M. (2018), "Evaluation of heaving resistance for deep shaft using nodular diaphragm wall", *Int J Geomech*., **14**(46), 40-45. https://doi.org/10.21660/2018.46.7265.

Watanabe, K., Sei, H., Nishiyama, T. and Ishii, Y. (2011), "Static axial reciprocal load test of cast-in-place nodular concrete pile and nodular diaphragm wall", *Geotech. Engi. J. SEAGS & AGSSEA*., **42**(2), 11-19.

Yokoyama, T., Suzuki, T. and Ito, A. (2009), "The new symbol of Tokyo: Underground diaphragm walls that support the Tokyo Sky Tree", *Cement Concrete*, (752), 9-13. (in Japanese)

Yu, J., Zhou, J., Zhang, R. and Gong, X. (2022), "Installation effects and behavior of a driven prestressed high-strength concrete nodular pile in deep saturated soft clay", *Int. J. Geomech*., **23**(3), 05022007. https://doi.org/10.1061/IJGNAI.GMENG-8130.

Yang, Y. and Qiu, L. (2020), "MPM simulation of uplift resistance of enlarged base piles in sand", *Soils Found*., **60**(5), 1322-1330. https://doi.org/10.1016/j.sandf.2020.08.003.

Zhou, J., Gong, X. and Zhang, R. (2019), "Model tests comparing the behavior of pre-bored grouted planted piles and a wished-in-place concrete pile in dense sand", *Soils Found*., **59**(1), 84-96. https://doi.org/10.1016/j.sandf.2018.09.003.

Zhou, J., Yu, J., Gong, X., El Naggar, H.M. and Zhang, R. (2021), "Field study on the behavior of pre-bored grouted planted pile with enlarged grout base", *Acta Geotech*., **16**, 3327-3338. https://doi.org/10.1007/s11440-021-01208-7.